Parametric comparison of selected dual elements PIR sensors

* Faisal Rafique, ** Najeeb Siddiqui

***Abstract*— Most of the warm blooded animals emanate thermal radiations in the MWIR to LWIR (Medium Wave to Long Wave Infrared) range from 3µm to 18µm. If the object is warmer than the surroundings, its thermal radiation is shifted toward higher frequency within the band and the thermal flux rate becomes stronger. To detect radiation in this band, single and multi-elements pyroelectric sensors utilized in the scanning systems to detect, with background contrast, the presence of still or moving thermal objects emitting thermal flux in the bandwidth specified. PIR sensors are commonly used to detect these radiation, their response is further process by electronic systems and generally analyze by software embedded systems. Here we present a comparative study of commercially available PIR sensors. In this study we evaluated dual element PIR sensors for their electrical and thermal parameters. Two types of test procedures were used, which can be used for any type of PIR sensors.**

***Index Terms*—Detectivity, Fresnel Zone, Heat Flux, Pyroelectric Infrared Sensor, Responsivity.**

I. INTRODUCTION

PIR (Pyroelectric or Passive Infrared) sensors are generally used to detect the presence of thermal radiating live sources for security purposes, while it has been successfully employed in fire detection and thermal gradient surveillance in various Fresnel zones [1], with accounted for sources at temperatures lower than Curie point of the pyro-sensitive substance. Most dielectric materials have a high thermal emissivity, while thermal emissivity of a warm blooded animal's skin is over 90% in MWIR (Medium Wave-Infrared) range. The output current *i* from a single element PIR sensor without gain can be calculated on the basis of the Stefan–Boltzmann Law [2]:

$$i \approx \left(\frac{2P\sigma a\gamma}{\pi hc}\right) bT_a^3 \left(\frac{T_b - T_a}{L^2}\right) \qquad (1)$$

Where T_b is the object temperature and the difference $T_b - T_a$ determines the temperature shift between the object and its background or ambient temperature, P is the pyro coefficient, σ is the Stefan-Boltzmann constant, a is the facet lens area, γ is the lens transmission coefficient, h is the thickness of the sensing element, and c is the specific heat of the pyroelectric element and L is the distance from sensing element to the object.

In equation (1) the first term in parenthesis characterizes the detector, while the rest relates to an object. The pyroelectric current *i* is directly proportional to the thermal contrast between the object and its background Field of View (FOV) and to the surface area of the object that confronts the detector. It is also dependent on the thickness of the sensing element; the thinner element produces heavy charge flow through the substrate that makes the detector more sensitive.

Pyroelectricity is an analogous physical process to piezoelectricity, in which a change in temperature causes thermal deformation of pyrosensitive material that generates charge carriers on the surface of the material [3]. The internal view of a dual element PIR sensor is shown in Figure-1. The pyro sensitive materials used in these PIR sensors are generally Lithium Tantalate ($LiTaO_3$), Lead Tantalate ($PbTaO_3$) Ceramic, Polyvinylidene Fluoride (PVDF), Deuterated Triglycine Sulfate (DTGS) and others, including their derivatives, which have high thermal responsivity compared to their piezo responses [2]. In Figure-1 a moving thermal radiant flux, with contrast, changes the dipole movement and generates substantial dielectric current across the first and then the second element that in turn generates a relaxation response signal as shown at the top of this figure. The slow relaxation is due to the very high impedance of hundreds of giga-ohms across these capacitive charge displacement substances, therefore their corresponding response time is too low in the range of mHz to few tens of Hz. A typical TO-5 PIR sensor's internal assembly with a high impedance FET based amplifier is shown in Figure-2.

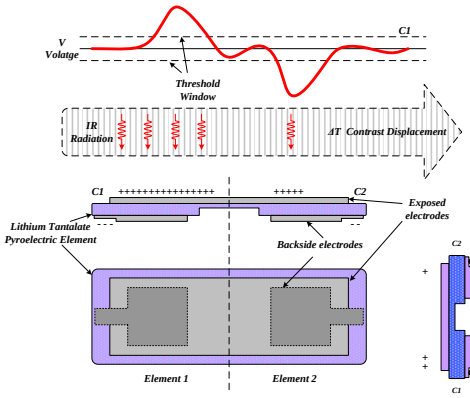

Figure 1:
Two Element PIR sensor internal view, charge formation due to differential thermal gradient field or due to thermal contrast and voltage waveform generation.

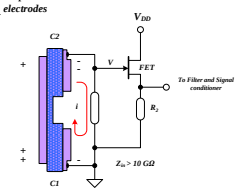

Figure 2:
A typical PIR sensor consists two resistors and one FET that act as a very high impedance high sensitivity amplifier. All these are embedded in a TO-5 metal package.

* Department of Applied Physics, University of Karachi. Email: faisal.rafique@uok.edu.pk
** Department of Electronic Engineering, Sir Syed University of Engineering & Technology, Karachi. Email: najeebs@ssuet.edu.pk

II. EVALUATION OF SENSORS

A suitable response of sensors must be tested before installing a sensor in a specific application. In advance applications these PIR sensors have been used for the detection of overheating industrial elements like actuators, solenoids, grid points etc. [1], in Flame detection [4], as a part of a biometric system [5] and IR thermometry, target tracking and angle-only measurements of the target from missile [6], in Intelligent system to distinguish humans from other warm blooded animals, tracking and detecting path dependent and independent gait recognition and classification systems [7-10].

In most of the scanning systems the parameters requirement is high in responsivity above 3 kV/W and high normalized detectivity D*, in the range of ~ 4-15µm wavelength, while low match, low offset and very low noise make the system conformity to true detection. The two initial test procedures will be conducted to verify the parameters given in the data sheets; one of the suitable sensor fall into requirements, will then be chosen to other practical application as was in [1].

SENSOR TEST-1

In this test procedure sensors tested with a basic experimental setup containing a Fresnel lens consisting of three arrays of 3, 4, and 5 lenses made from POLY-IR 2 [11] material. Two sensors D203 and LHI968 have been chosen. Experimental bench includes a lock-in amplifier, chopper, fixed 75dB gain and variable gain amplifiers, a thermal IR source and an interfaced DAQ to a PC.

A setup for measuring initial response of D203B and LHI968 is shown in Figure-3. The selected sensors have filter-less spectral range from visible to over 50µm, while an IR filter limits its range from 5.5µm - 14µm and its response is higher than 3300 V/W which falls in our research requirement parametric range. In this procedure radiation from a hot object having surface temperature of 150ºC, less than the Curie temperature, with projected surface area of 3 sq-inch passes in front of FOV of the Fresnel Zone-1 at a distance of four feet while other zones were masked. Three basic responses were observed in this setup, as shown in Figure-4:

1) In insert (a), when equal heat flux passes across the Fresnel zone-1 (red and blue in Figure-3).In this case each element in PIR sensor produces equal and opposite response because elements are connected in series.
2) In insert (b), unequal heat flux in partial Fresnel zone. In this case one element has more twisted dipole response than other, thus produces unequal and opposite responses.
3) In insert (c), equal heat flux falls on both the partial Fresnel zones (red and blue), produces equal and opposite responses from each element at the same time,it is thus cancelled.

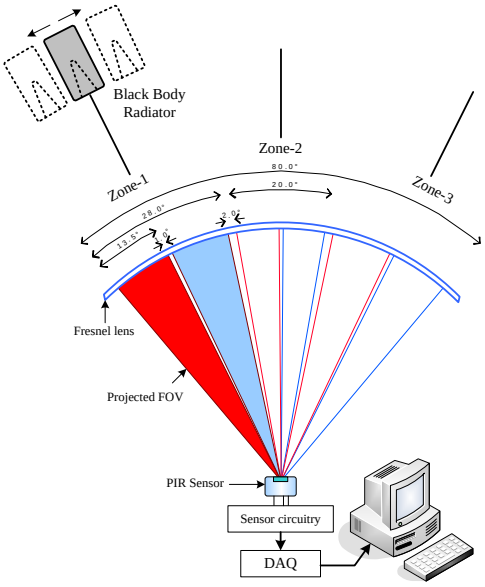

Figure-3: Basic Test Setup

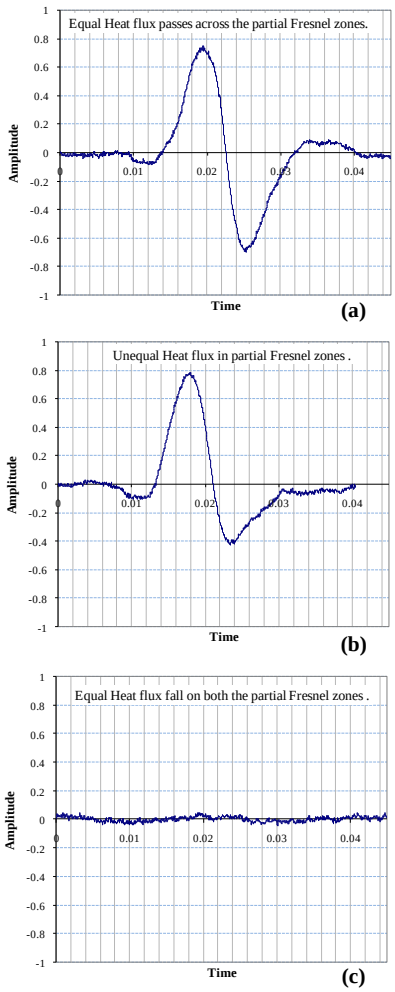

Figure-4: D203B normalized responses with gain.

Both the sensors tested for the basic responses and have been found almost the same behavior for the thermal stimulus, only the results of D203B shown in Figure-4. Both sensors enclosed in a TO-5 anti-erode metal housing that protects the internal circuitry and elements, but it should be treated as a MOS device. An infrared window filter protects the elements from strong white light disturbance and defines the response range in MIR band of the spectrum. PIR sensors have some important physical parameters that characterize its degree of performance. These parameters of D203B and LHI968 sensors provided by the manufacturers are given in the Table-1, that includes Responsivity, Match or Balance, NEP, Directivity (D-parameter) and Noise. Generally the output of such type of detectors ranges from above noise floor to few tenths of millivolts depending on the target temperature and temperature contrast with background of the target source, modulating frequency, and the distance from the source without focusing apparatus.

Table-1: Physical parameters provided by manufacturers.

Parameter	DS203B		
	Range	Unit	Condition
Responsivity	>3.3	kV/W	147ºC, 1Hz, Δf = 0.3-3.5Hz
Match	<10%	V/W or %	
Offset	0.3-1.2	V	25ºC, Rs = 47k
Noise	<70	mVpp	25ºC
Nor-Detectivity D*	≥1.4 ×10^8	cmHz$^{1/2}$/W	147ºC, 1Hz
Supply	3-15	V	-
FOV	Ver~110º Hor ~110º	Degrees	-
Operating & Storage Temp	-40 to 80	ºC	-

Parameter	LHI968		
	Range	Unit	Condition
Responsivity	3.3 - 3.8 (typ)	kV/W	100ºC, 1Hz, Δf = 0.3-3.5Hz
Match	< 0.33 (1% typ -10%)	V/W or %	-
Offset	0.2-1.5	V	25ºC, Rs = 47k
Noise	20 typ – 50	µVpp	25ºC, Δf = 0.3-10Hz
Nor-Detectivity D*	5×10^7 - 19×10^7	cmHz$^{1/2}$/W	100ºC, 1Hz, BW= 1Hz
Supply	2-15	V	25ºC, Rs = 47k
FOV	Ver 100º Hor 100º	Degrees	Unobstructed
Operating & Storage Temp	-40 to 80	ºC	-

(i) Responsivity

It is defined as the sensor response related to the incident radiation. Responsivity is the RMS output voltage, VRMS, or RMS current response, IRMS, per unit incident RMS radiant energy ψ_{RMS} at given chopping frequency and bandwidth for a defined black body radiator. Reponsivity units are Volts/Watt (V/W) or Ampere/Watt (A/W). For multi element sensors it is measured for each element separately. Mathematically it is written as:

$$R(\lambda, f) = \frac{|V_{RMS}|}{\psi_{\lambda,RMS}} \quad (2a) \qquad R(\lambda, f) = \frac{|I_{RMS}|}{\psi_{\lambda,RMS}} \quad (2b)$$

The spectral responsivity is maximum at the low chopping frequency; generally it is measured at 1Hz for motion detection and 10Hz for range measurements and has maximum value at approximately 0.1 Hz. In equation (2) λ indicates the response measured at specific wavelength or spectral range Δλ while *f* indicates the chopping frequency. We can write Spectral or closed monochromatic Responsivity as:

$$R(\lambda, f) = \frac{|V_{RMS}|}{\psi(\lambda)\Delta\lambda} \quad (2c)$$

While for a perfect Blackbody radiator we should integrate over whole spectral range i.e.

$$R(\lambda, f) = \frac{|V_{RMS}|}{\int_0^\infty \psi(\lambda) d\lambda} \quad (2d)$$

The spectral and blackbody responsivity almost remains same for a sensor having spectral filter window with very small reflectance. There are different radiation sources that produce single wavelength or very narrow wavelength radiation; includes monochromators, tunable lasers, and optical filters.

In measuring spectral responsivity; prisms and diffraction gratings are used to extract monochromatic radiation flux ψ_λ from a blackbody radiation flux ψ_{BB} that passes through a stop-exit slit and falls onto the sensor surface, in this case the responsivity can be calculated directly from equation (2). For measuring spectral responsivity the test procedure is depicted in Figure-5. The actual test bench included a Gray body radiator, chopper, sensor under test, occluder, lock-in amplifier, and data acquisition setup.

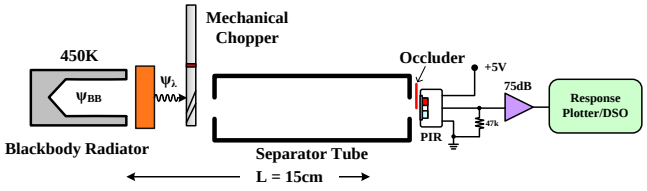

Figure-5: Measuring spectral responsivity.

(ii) Balance

Balance is another very important performance counting parameter for multi element PIR sensors. The balance or match compares the responsivity match of each element, ideally it should be zero and practically it should not be greater than 10% of the minimum responsivity value. It can be specified either in responsitivity unit (V/W) or in percentage of responsivity.

The Match value of a dual element sensor can be calculated from the individual element sensitivity level; if E_A and E_B are

the sensitivity levels then Match can be calculated from following equation:

$$Match = \frac{E_A - E_B}{E_A + E_B} \quad (3)$$

There are two methods to measure Match, in the first method an occluder is used to block one element and excitation is measured across element's electrode. With the same IR source the procedure repeated for the second element. In the second method a mechanical chopper with occluders are used and excitation is measured from sensor's electrodes.

(iii) Noise

There are three sources of noises in the test circuit:

A. The noise generated by pyroelectric substance itself.
B. The noise due to ohmic path especially in high value resistors is considerable.
C. The noise of the internal FET.

The dynamic range of the sensor is affected by noise, in ferroelectric/pyroelectric substances the noise decreases in the frequency range of 2-50Hz. It is measured in µVpp with specified test conditions including operating temperature and chopping frequency.

(iv) Noise Equivalent Power (NEP) and Normalized Detectivity (D)*

Another figure of merit to compare different sensors is NEP and Detectivity. It gives Noise-Bandwidth related figures that also reflect noise contents generated by sensor and it's supporting embedded electronic circuitry. The basic unit of NEP is Watt but it can also be referenced to a fixed electrical bandwidth, thus in the case unit specified in Watts per square-root Hertz (W/Hz$^{1/2}$).
For a sensor specified NEP value corresponds to the minimum radiation to be detected by the sensor that produces output that exceeds the noise level. In practical applications the theoretical minimum detectable power W_m at absolute temperature T and bandwidth Δf is given as:

$$W_m^2 = 16A\sigma kT^5\Delta f \quad (4)$$

The square root of $16A\sigma kT^5$ quantity in (4) is called NEP, thus we can write:

$$NEP = \frac{W_m}{\Delta f^{1/2}} = \sqrt{16A\sigma kT^5} \quad (5a)$$

Practically we can calculate NEP by measuring responsivity level R_v, and noise level N_v, where R_v can be calculated by measuring sensor voltage level change ΔV_s caused by incident radiant flux drift $\Delta\psi_s$,thus in this case we have:

$$NEP = N_v \frac{\Delta\psi_s}{\Delta V_s} \quad (5b)$$

or

$$NEP = \frac{N_v}{R_v} \quad (5c)$$

Small value of NEP indicates better sensor. Usually when the performance increases then it implies that its magnitude increases, thus another figure of merit is defined which is just the reciprocal of NEP is called Detectivity denoted by *D*, defined as:

$$D = \frac{1}{NEP} \quad (5d)$$

For many detectors W_m is proportional to the square root of the area A and square root electrical bandwidth, thus the normalized NEP (denoted by NEP*) is the NEP value divided by $A^{1/2}$ and $\Delta f^{1/2}$ and Normalized Detectivity (denoted by D*) is the reciprocal of NEP*, mathematically written as:

$$D^* = \frac{1}{NEP^*} = \frac{\Delta f^{1/2} A^{1/2}}{NEP} \rightarrow m / W_m \sqrt{Hz} \quad (6)$$

The normalized values of *NEP* and *D* enable us to compare different sensors of same material independent of their surface area. Unit of D* is cmHz$^{1/2}$W^{-1}.

SENSOR TEST-2

This test procedure measures parameters of the selected sensors LHI968 and D203B, exactly defined in standard test bench procedure. Selected parameters include; Responsivity, Noise level, NEP and D*.
The experimental setup is shown in Figure-6 that is a Band-limited radiation pyrometer; it includes a heat source, mechanical chopper, adjustable gain amplifier with 75dB maximum output, shutter and occluder. Shutter is used for noise measurement while occluder can block one of the PIR elements for the measurements of responsivity and match. For chopping the FOV, a geared motor and RPS counter was used.
In this test, filter method is used to pass through radiation of specific wavelength range. Without any filter the 60% sensor responsivity is observed from visible to 50 µm. For the given sensors, the IR filter window is highly transmissive in ~5-14 micrometer wavelength; the spectral response of LHI968 with standard filter window is shown in graph Figure-7, provided by the manufacturers. Other narrow band filter is also available to cover mid-IR range.

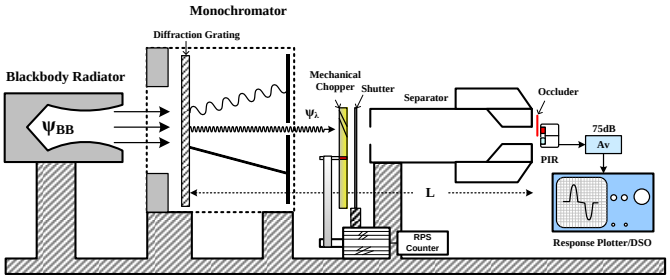

Figure-6: Filter Method. In this test the radiator source at 450K emit wide wavelength in IR and visible. IR filter at the sensor is highly transmissive in the range ~5 to 14μm.

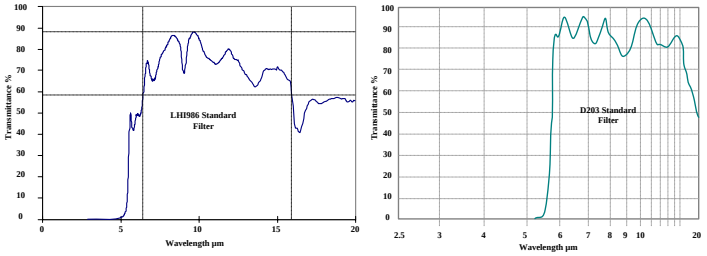

Figure-7: Sensor response with IR filter. (Plots provided by PerkinElmer and PIR Sensor Co.)

III. MEASUREMENTS AND CALCULATIONS

i- Responsivity

Parameters from data sheet:

FOV_H = 110º (Hor) [55º/element]
FOV_V = 120º (Hor) [60º/element]
Sensor's Element Area = 2mm/element [2×1mm2]

Measuring Conditions:

Chopper frequency f_{ch} = 10 Hz.
Blackbody temperature T_{BB} = 500K.
Sensor temperature T_S = 25ºC (Ambient).

The radiant fluxes at 298K (Ambient) and 500K (Gray Body) can be computed using Stefan-Boltzmann law based on FOV:

$$\psi = \frac{1}{2}\varepsilon A\sigma T^4 Sin^2(FOV) \qquad (7)$$

Where

ε is the emissivity which is a unit less quantity (in present case we consider close value of 0.98).
A is the area of individual sensor's element.
T is the absolute temperature.
σ is Stefan-Boltzmann constant.
FOV is the Field of vision in degrees.

The measured voltages E_A or V_{pA} (element-1) and E_B or V_{pB} (element-2) corresponds to each single element by using occluder to block alternate element and measured voltage value for both the elements V_{pp} without occluder are:

LHI968:

V_{pA} = 8.6577/2 = 4.32885V
V_{pB} = 8.6506/2 = 4.3253V
V_{pp} = 17.3166/2 = 8.6583V

$V_{RMS/A}$ = 3.0609V
$V_{RMS/B}$ = 3.0584V
V_{RMS} = 3.0611V

DS203:

V_{pA} = 7.3512/2 = 3.6756V
V_{pB} = 7.9324/2 = 3.9662V
V_{pp} = 15.4256/2 = 7.7128V

$V_{RMS/A}$ = 2.5990V
$V_{RMS/B}$ = 2.80455V
V_{RMS} = 2.7268V

When an element is blocked by chopper or by occluder the ambient temperature is considered as the second blackbody temperature. If element's FOV is 55 degrees, then using (7) at 298K the radiant power is:

$$\psi(298K) = 0.98\left(2\times10^{-3}\right)^2 5.67\times10^{-8}298^4 Sin^2\left(\frac{55}{2}\right) = 373.72\mu W$$

When sensor's element sees the blackbody at 500K, the radiant power in the FOV of 55 degrees is:

$$\psi(500K) = 0.98\left(2\times10^{-3}\right)^2 5.67\times10^{-8}500^4 Sin^2\left(\frac{55}{2}\right) = 2961.83\mu W$$

The peak-to-peak flux is just the difference of fluxes at 300K and 500K:

$$\psi_{pp} = \psi(500K) - \psi(298K) = 2961.83\mu W - 373.72\mu W$$
$$\Rightarrow \psi_{pp} = 2588.11\mu W$$

The steady component of chopped radiant flux, average radiant flux and effective (RMS) radiant flux dependent on the peak-to-peak values:

$$\psi_o = \frac{1}{2}\psi_{pp} = 1294.055\mu W$$
$$\psi_s = \frac{2}{\pi}\psi_{pp} = 1647.64\mu W \text{ and}$$
$$\psi_s = \psi_{\lambda,RMS} = \frac{1}{2}\psi_s = 823.82\mu W$$

Note that in a non steady measurement for a pyroelectric element the steady component of the chopped radiant flux does not correspond to any change in the output signal but rather increases the temperature of the element surface, also it does not correspond to the mean temperature change between blackbody and surface of the pyro element. Now the Responsivity can be calculated using equation (2a):

$$\overbrace{R(500K,10Hz)_{element1} = \frac{|V_{RMS}|}{\psi_{\lambda,RMS}} = \frac{3.0609\text{V}}{823.82\mu W} = 3715.49V/W}^{LHI968}$$

$$R(500K,10Hz)_{element2} = \frac{|V_{RMS}|}{\psi_{\lambda,RMS}} = \frac{3.0584\text{V}}{823.82\mu W} = 3712.46V/W$$

$$R(500K,10Hz)_{dual} = \frac{|V_{RMS}|}{\psi_{\lambda,RMS}} = \frac{3.0611\text{V}}{823.82\mu W} = 4383.23V/W$$

$$\overbrace{R(500K,10Hz)_{element1} = \frac{2.5990\text{V}}{823.82\mu W} = 3154.81V/W}^{DS203}$$

$$R(500K,10Hz)_{element2} = \frac{2.80455\text{V}}{823.82\mu W} = 3404.32V/W$$

$$R(500K,10Hz)_{dual} = \frac{2.7268\text{V}}{823.82\mu W} = 3309.94V/W$$

ii- Match/Balance

As a standard Element Match value should not be greater than ten percents of the minimum Responsivity value. In the measurement setup second method was used to measure Match value. Using relation (3) we have:

$$Match_{LHI968} = \left|\frac{E_A - E_B}{E_A + E_B}\right| = \left|\frac{4.32885 - 4.3253}{4.32885 + 4.3253}\right| = 4.102078\times10^{-04} \text{ or } 0.041\%$$

$$Match_{DS203} = \left|\frac{E_A - E_B}{E_A + E_B}\right| = \left|\frac{3.6756 - 3.9662}{3.6756 + 3.9662}\right| = 3.802768\times10^{-02} \text{ or } 3.8\%$$

iii. Noise

For noise measurements, shutter is closed to block all radiations to the sensor. The noise signals generated have various sources and have cumulative result that includes noise from sensor material, due to high value ohmic paths and from built in FET in PIR sensor body. Table-2 shows noise measurement conducted in random instances for 20, 25, and 50 seconds at 25ºC.

Table-2: Average RMS noise measurement results.

LHI968 Noise in $\mu V_{pp\ (max)}$			**DS203B Noise in $\mu V_{pp\ (max)}$**		
20 sec	**25 sec**	**50 sec**	**20 sec**	**25 sec**	**50 sec**
26	24	22	43	34	34
32	32	41	41	54	54
26	27	28	56	67	64
26	36	35	45	43	82
26	28	29	64	66	43
Average RMS Noise Voltages $VRMS_{Avg}$ (N_v)					
9.61	**10.39**	**10.96**	**17.60**	**18.66**	**19.58**

iii- NEP

From previous measurements of noise levels and responsivities for dual elements at 500K and 10Hz chopping frequency, using (5c), the NEP found to be:

$$NEP(LHI968) = \frac{N_v}{R_v} = \frac{10.96\mu}{4383.23} = 2.5004nW$$

$$NEP(DS203) = \frac{N_v}{R_v} = \frac{19.58m}{3309.94} = 5.9155\mu W$$

For 1Hz bandwidth as in our case:

$$D^*(LHI968) = \frac{1}{NEP^*} = \frac{1^{1/2}4^{1/2}}{2.5004nW} = 7.99\times10^{8} m/W_m\sqrt{Hz}$$

$$D^*(DS203) = \frac{1}{NEP^*} = \frac{1^{1/2}4^{1/2}}{5.9155\mu W} = 3.38\times10^{5} m/W_m\sqrt{Hz}$$

IV. RESULTS

All of the measured parameters in test setup-2 for the selected sensors are tabulated in Table-3.

Table-3: Measured parameters of specific PIR modules.

Parameter	**DS203B**				
	Range	**Test Condition**	**[b]Measured**	**Test Condition**	**Units**
R_v	>3.3	450K, 10Hz	**3.309**	500K, 10Hz	kV/W
Match	<10%		**3.8%**		V/W or %
Offset	0.3-1.2	25ºC, R_s = 47k	-	25ºC, R_s = 47k	V
Noise	<70m	25ºC	**19.58μ**	25ºC, Δf = 10Hz	V_{pp}
D*	≥1.4 ×10^8	150ºC, 1Hz	**3.38×10^7**	500ºC,1Hz, BW = 1Hz	cmHz$^{1/2}$/W

	LHI968 (Unit marked-1)				
	Range	**Test Condition**	**Measured**	**Test Condition**	**Units**
R_v	3.3 - 3.8 (typ)	450K, 10Hz	[a]**3.339** [b]**4.383**	500K, 10Hz	kV/W
Match	< 0.33 (1% typ10%)	-	[a]**0.04%** [b]**0.01**	-	V/W or %
Offset	0.2-1.5	25ºC, R_s = 47k	[b]**0.77**	25ºC, R_s = 47k	V
Noise	20 typ - 50	25ºC, Δf = 0.3-10Hz	[a]**10.96**	25ºC, Δf = 10Hz	μV_{pp}
D*	5×10^7 - 19×10^7	100ºC,1Hz, BW = 1Hz	[a]**7.99×10^{10}**	500ºC,1Hz, BW = 1Hz	cmHz$^{1/2}$/W

a) Measurements for specific PIR module [unit-1] provided by manufacturer.
b) Test Measurements for PIR modules.

V. CONCLUSION

Two types of experimental tests were performed on commercially available PIR sensors. From the evaluation tests both sensors (LHI968 and DS203) have been found responsivity greater than 3100 V/W (for DS203) and 3700 V/W (for LHI968), low noise, low percent match and low offset voltages. Ascertaining results agree with the manufacturer's measurements and indicate that LHI968 (unit marked.1) is better than DS203 unmarked sample used.

ACKNOWLEDGMENT

Authors are thankful to Perkin Elmer for providing specific parameters value of each sensor of LHI968 model.

VI.REFERENCES

[1] F. Rafique and N. Siddiqui "Passive IR field detection of thermal objects in active Fresnel zones", Infrared Physics & Technology, 60(2013) 145-154.http://dx.doi.org/10.1016/j.infrared.2013.04.00

[2] J. Fraden, Handbook of Modern Sensors, 2nd ed., Woodburg, NY, AIP Press, 1997.

[3] Sensor Technology Handbook by Jon. S. Wilson. Elsevier, ISBN: 0-7506-7729-5

[4] B. Ugur Toreyin, et al."Flame detection system based on wavelet analysis of PIR sensor signals with an hmm decision mechanism". 16th European signal processing Conference (EUSIPCO 2008), Lausanne, Switzerland, 25th August 2008.

[5] Jian-Shuen Fang,, Qi Hao, , David J. Brady, Bob D. Guenther, Ken Y. Hsu. "A pyroelectric infrared biometric system for real-time walker recognition by use of a maximum likelihood principal components estimation (MLPCE) method". 19 March 2007 / Vol. 15, No. 6 / Optics Express 3271.

[6] Goran Dikic, Branko Kovacevic, "Target Tracking with Passive IR Sensors", TELSIKS 2001, 19-21 September 2001, NiS, Yugoslavia.

[7] Jian-Shuen Fang, Qi Hao, David J. Brady, Mohan Shankar, Bob D. Guenther, Nikos P. Pitsianis, Ken Y. Hsu "Path-dependent human identification using a pyroelectric infrared sensor and Fresnel lens arrays", Jan 2006/Vol. 14, No. 2/OPTICS EXPRESS.

[8] Mohan Shankar, John B. Burchett, Qi Hao, Bob D. Guenther, David J. Brady, "Human-tracking systems using pyroelectric infrared detectors", Optical Engineering 106401-1 October 2006/Vol. 45(10).

[9] F. Xu and K. Fujimura, "Pedestrian detection and tracking with night vision," in Proc. IEEE Intelligent Vehicle Symp. 2002.

[10] R. Bodor, B. Jackson, and N. Papanikolopoulos, "Vision-based human tracking and activity recognition," in Proc. 11th Mediterranean Conf. on Control and Automation 2003.

[11] Fresnel Technologies Inc., http://www.fresneltech.com.